PERFORMANCE-BASED STUDY OF LONG-SPAN STEEL–CONCRETE COMPOSITE TRUSSES FOR HIGH-RISE STRUCTURES

My PHAM*

The University of Danang - University of Science and Technology, Vietnam

*Corresponding author: pmy@dut.udn.vn

(Received: May 02, 2025; Revised: June 10, 2025; Accepted: June 23, 2025)

DOI: 10.31130/ud-jst.2025.23(10C).672E

Abstract - This study presents a comprehensive evaluation of long-span steel–concrete composite trusses for high-rise buildings, integrating Eurocode-based theoretical analysis with finite element modeling (FEM). A performance-based design methodology is proposed, enabling efficient cross-section selection during the construction stage. This approach not only enhances structural efficiency and serviceability but also significantly reduces design iterations and construction complexity. The close agreement between analytical and numerical results confirms the reliability of the proposed method and reinforces its applicability to real-world projects. The findings provide valuable insight into the structural behavior of composite trusses and establish a robust foundation for their broader use in high-rise applications demanding performance-driven and material-efficient solutions.

Key words - Steel–concrete composite truss; Long-span structures; High-rise buildings; Performance-based design; Finite element method (FEM); Structural optimization; Eurocode; Load-bearing capacity.

1. Introduction

The rising demand for high-rise buildings has driven the evolution of efficient, lightweight structural systems. Steel–concrete composite trusses, which integrate steel chords with concrete webs or slabs, offer notable advantages over traditional steel trusses, including enhanced strength-to-weight ratios, improved fire resistance, and greater architectural adaptability.

Recent research underscores the benefits of long-span composite trusses in reducing story heights, minimizing dead loads, and facilitating the integration of building services. Studies by Shen et al. [1], Xu et al. [2], and Duratna et al. [3] have demonstrated notable improvements in flexural and seismic performance. Chen and Liew [4] further advocate for performance-based design methods tailored to composite structures.

In modern high-rise designs, rooftop areas often demand long, column-free spans to accommodate mechanical equipment, green spaces, or communal areas. Composite trusses address these needs by supporting substantial loads while preserving open architectural layouts. Unlike traditional deep beams requiring web openings, composite trusses offer seamless service integration without compromising structural integrity.

Tan et al. [5] and the Steel Construction Institute [6] emphasize the versatility of composite trusses in multifunctional spaces, while Ali and Al-Kodmany [7] reaffirm their relevance in tall building systems.

Despite their potential, research on composite trusses remains limited due to the lack of dedicated design standards, complex mechanical behavior, limited experimental data, and practical challenges in fabrication and assembly. This study addresses this gap by evaluating the structural performance of long-span steel–concrete composite trusses using both analytical and FEM approaches. The results provide a comparative analysis with conventional steel trusses under Eurocode standards, supporting broader adoption in high-rise construction.

2. Material properties of the composite system

The performance of steel–concrete composite trusses is fundamentally governed by the mechanical and thermal properties of their constituent materials - namely concrete, reinforcing steel, structural steel, and profiled steel sheeting.

Concrete properties follow the provisions of Eurocodes EC2 and EC4, covering strength classes from C20/25 to C50/60. Both normal-weight ($1800 \leq \rho \leq 2500\ kg/m^3$) and lightweight ($1600 \leq \rho \leq 1800\ kg/m^3$) concretes are applicable. Key mechanical properties include compressive strength ($\mathrm{f_{ck}}$), tensile strength ($\mathrm{f_{ctm}}$), modulus of elasticity ($\mathrm{E_{cm}}$), and characteristic tensile strength ($\mathrm{f_{ctk,0.05}}$). Design values are determined as follows:

- Compressive strength: $f_{cd} = \alpha_{cc} \cdot f_{ck}/\gamma_c$;
- Tensile strength: $f_{ctd} = \alpha_{ct} \cdot f_{ctk,0.05}/\gamma_c$.

Note that α_{cc} and α_{ct} account for long-term effects and unfavorable loading on compressive and tensile strengths, respectively. These values vary by country but are typically taken as 1.0. The modulus of elasticity is adjusted based on aggregate type and concrete density. For composite section analysis, the modular ratio is applied as: $n = E_s/E_{cm}$.

The thermal expansion coefficient of concrete is nearly equal to that of structural steel, ensuring compatibility under temperature variations. Their typical values are:

- $\alpha = 10^{-5}\,{}^0C^{-1}$ for normal-weight concrete and steel;
- $\alpha = 10^{-7}\,{}^0C^{-1}$ for lightweight concrete.

Steel reinforcement consists of hot-rolled rebars complying with EN 10080, most commonly in grades S220, S400, and S500, characterized by their yield strength f_{sk} and a standard modulus of elasticity (E_s) of 210 GPa. Structural steel used in truss members typically follows EN 1994-1-1 standards and includes grades S235, S275, and S355, with yield stress (f_y) values dependent on the cross-sectional thickness.

Profiled steel sheeting is specified per EN 10147, with a yield strength (f_{yp}) of 280–350 MPa and a thickness (t) range of 0.7–1.2 mm. A zinc coating of approximately 0.02 mm provides enhanced corrosion resistance and durability.

3. Design of steel-concrete composite trusses

In the design of steel–concrete composite trusses, the effective width of the concrete slab is a critical factor influencing structural performance. Accurately defining this width ensures proper load distribution, stiffness, and stability. When appropriately accounted for, it enhances strength, durability, and material efficiency, allowing composite trusses to achieve optimal performance in modern construction.

3.1. Effective width of concrete slabs

The effective width of the concrete flange is determined in accordance with Eurocode 4 [8], as outlined in Table 1 and illustrated in Figure 1.

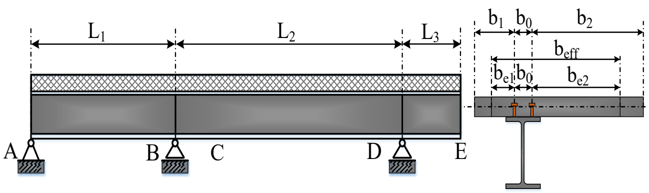

Figure 1. *Diagram illustrating the calculation of the effective width of the concrete flange*

Table 1. *Formula for determining the effective influence width of the concrete flange in composite trusses*

Location	Effective Flange Width Formula	Applicable standards
Pinned support A	$b_{eff} = b_0 + \sum \beta_i \cdot b_{ei}$	Expression (5.4), EN 1994-1-1
	$\beta_i = \left(0.55 + 0.025\frac{L_e}{b_{ei}}\right) \leq 1.0$	Expression (5.5), EN 1994-1-1
	$L_e = 0.85L_1$	Figure (5.1), EN 1994-1-1
Span AB	$b_{eff} = b_0 + \sum b_{ei}$	Expression (5.3), EN 1994-1-1
	$b_{ei} = \frac{L_e}{8} \leq b_i$	-
	$L_e = 0.85L_1$	Figure (5.1), EN 1994-1-1
Roller support BC	$b_{eff} = b_0 + \sum b_{ei}$	Expression (5.3), EN 1994-1-1
	$b_{ei} = \frac{L_e}{8} \leq b_i$	-
	$L_e = 0.25(L_1 + L_2)$	Figure(5.1), EN 1994-1-1
Span CD	$b_{eff} = b_0 + \sum b_{ei}$	Expression (5.3), EN 1994-1-1
	$b_{ei} = \frac{L_e}{8} \leq b_i$	-
	$L_e = 0.7L_2$	Figure (5.1), EN 1994-1-1
Roller support DE	$b_{eff} = b_0 + \sum b_{ei}$	Expression (5.3), EN 1994-1-1
	$b_{ei} = \frac{L_e}{8} \leq b_i$	-
	$L_e = 2.0L_3$	Figure (5.1), EN 1994-1-1

3.2. Classification of steel truss systems in composite structures

Various truss geometries are used in composite systems, typically selected based on structural efficiency and material economy. The Pratt truss (Figure 2a), characterized by tensioned diagonals and short compression verticals, optimizes steel's tensile strength but can be material-intensive and limit service integration. In contrast, the triangular Warren truss (Figure 2b) offers reduced material use and improved clearance. Its performance improves when modified into a Vierendeel-type configuration with horizontal intermediate members (Figure 2c), enhancing serviceability across the truss depth. The most efficient configuration incorporates two parallel intermediate members and a sloped bottom chord (Figure 2d). However, the number and arrangement of diagonals remain critical to structural integrity.

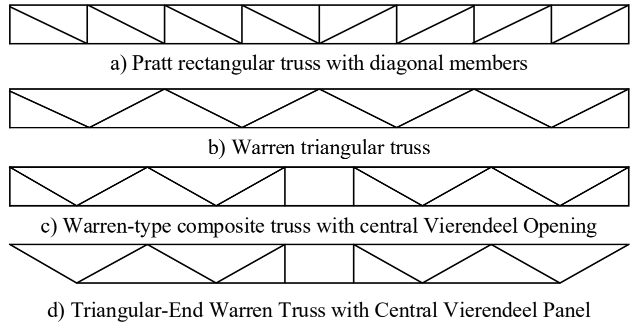

Figure 2. *Common types of steel truss systems used in steel-concrete composite structures*

3.3. Working mechanism diagram of steel-concrete composite trusses

This study analyzes a composite truss spanning between two columns, subjected to a uniform load and designed in accordance with Eurocode 4 [8-10]. This system efficiently concentrates material where internal forces are highest, minimizing overall consumption. Its open structure facilitates the routing of services without compromising performance, unlike deep-beam systems that require web openings [11, 12].

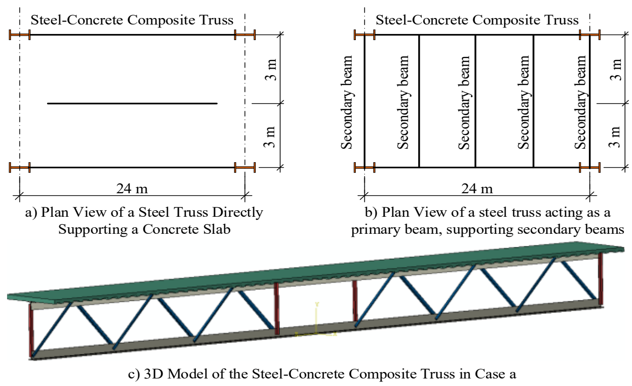

Figure 3. *Working mechanism diagram of steel-concrete composite trusses*

In high-rise applications, composite trusses commonly operate in two configurations: (i) with a steel truss directly supporting the concrete slab (Figure 3a), forming a fully integrated composite system, and (ii) with the steel truss acting as a primary beam supporting secondary beams and slabs (Figure 3b). This study focuses on the first configuration, modeled as a three-dimensional system shown in Figure 3c.

3.4. Structural requirements and analysis scheme

3.4.1. Structural requirements

Truss height typically ranges from 1/15 to 1/20 of the span, based on load conditions and architectural needs. Clearance of 150–250 mm beneath the truss is needed for lighting, fire protection, and service installations. Diagonal members are inclined at 30°–60°, with 45° being optimal for triangular units. In Vierendeel configurations, spacing between intermediate chords is limited to about 2.0 times the truss height

Top chord requirements include:

- Short segment subdivision to support construction loads;
- Minimum width of 120 mm;
- Minimum thickness of 8 mm;
- Capacity to resist moments induced by intermediate chords.

The adopted configuration is a modified Warren truss with a central Vierendeel panel (Figure 2c), spanning 21 meters with hinged supports (Figure 8). Node spacing is 2–3 meters, with 1.5–3 meters vertical distance between chords.

3.4.2. Load Cases and Structural Verification

Composite trusses operate in two stages:

- **Construction stage**: The steel truss alone supports its self-weight, fresh concrete, reinforcement, and live construction loads.
- **Service stage**: The hardened slab and steel chords form a composite section, enhancing strength and efficiency.

Structural checks include:

- Global bending capacity.
- Axial capacity of diagonal members.
- Number of required shear connectors.
- Local bending resistance of intermediate panels.

3.5. Structural verification of steel–concrete composite trusses

This section presents the essential structural verifications required to ensure the safe and reliable performance of steel–concrete composite trusses under various loading conditions.

3.5.1. Global Bending Capacity

The flexural resistance is evaluated based on the plastic stress distribution across the cross-section. The tensile capacities of the top and bottom steel chords are calculated from the yield strength of steel (f_y) and the corresponding cross-sectional areas (A_t and A_b):

$$\begin{cases} F_{AB} = \dfrac{f_y A_b}{\gamma_{M0}} \\ F_{AT} = \dfrac{f_y A_t}{\gamma_{M0}} \end{cases} \tag{1}$$

The compressive resistance of the concrete flange is determined using:

$$F_C = \frac{0.85 f_{ck}}{\gamma_c} b_{eff} h_c \tag{2}$$

where γ_c is the partial safety factor for concrete (typically 1.5), f_{ck} is the characteristic compressive strength of concrete (from cylinder tests), b_{eff} is the effective flange width, h_c and is the height of the concrete slab. The remaining parameters are illustrated in Figure 4.

In most cases, the axial force in the steel chords $F_a = F_{AB} + F_{AT} < F_C$ is less than the concrete compressive force F_C, indicating that the neutral axis lies within the concrete flange. Consequently, the plastic bending capacity of the composite truss is governed by the tensile force in the bottom chord, with the lever arm measured to the resultant compressive force in the concrete slab:

$$M^{+}_{pl,Rd} = F_{AB}\left(H_t + z_t + h_p + h_c - z\right) + F_{AT}\left(z_t + h_p + h_c - z\right) \tag{3}$$

In this context, z represents the position of the plastic neutral axis of the cross-section relative to the top surface of the composite reinforced concrete slab (see Figure 4). The expression for determining zzz is provided in Eq. (4).

$$z = \frac{\left(F_{AB} + F_{AT}\right)}{\dfrac{0.85 \cdot f_{ck}}{\gamma_c} b_{eff}} \tag{4}$$

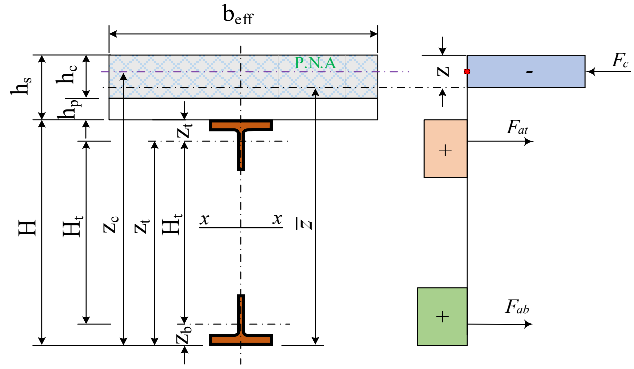

Figure 4. *Plastic stress diagram of the cross-section when the neutral axis passes through the concrete flange*

3.5.2. Deflection Check

The composite truss is modeled as a simply supported beam, and deflection is evaluated in two distinct stages:

- Construction Stage: At this stage, the concrete has not yet hardened, and therefore the deflection occurs solely in the steel truss without any contribution from the concrete slab. The deflection is mainly caused by the self-weight of the steel truss, the weight of the fresh concrete, and any live loads during construction. The deflection, denoted as δ_1, is calculated using Eq. (5) and checked against the construction-stage limit $\delta_1 \le l/250$.

$$\delta = \frac{5ql^4}{384E_s I_{xx}} \tag{5}$$

- Service Stage: After the concrete has hardened, composite action between the slab and steel truss is considered. The effective moment of inertia (I_{eq}) is calculated based on the transformed section properties, as given by:

$$I_{eq} = I_t + A_t\left(z_t - \bar{z}\right)^2 + I_b + A_b\left(z_b - \bar{y}\right)^2 + I_c^{eq} + A_c^{eq}\left(z_c - \bar{z}\right)^2 \tag{6}$$

Here, I_t and I_b and represent the moments of inertia of the top and bottom chords, respectively, while I_c^{eq} is the equivalent moment of inertia of the concrete flange transformed into steel. It is determined using:

$$I_c^{eq} = \frac{b_{eff} h_c^3}{12 n_{eq}} \tag{7}$$

To evaluate the deflection, Eurocode 4 guidelines are followed, using the equivalent cross-section properties.

According to Eurocode 4, the parameters in Eqs. (6) and (7) are computed as in Eq. (8). Where, b_{eff} is the effective width of the concrete slab, determined according to EC4 provisions (see Section 3.1); h_c is thickness of the concrete slab above the steel deck crest; A_t and A_b are area of top and bottom chords respectively; z_t, z_b and z_c are distances from the base to the centroids of top chord, bottom chord, and concrete flange (after conversion) as presented in Figure 4.

$$\begin{cases} n_{eq} = \dfrac{E_s}{E_{cm}} \\ \overline{z} = \dfrac{A_t z_t + A_b z_b + A_c^{eq} z_c}{A_t + A_b + A_c^{eq}} \\ A_c^{eq} = \dfrac{A_c}{n_{eq}} = \dfrac{b_{eff} \cdot h_c}{n_{eq}} \end{cases} \quad (8)$$

Finally, the total deflection of the composite steel–concrete truss system is determined using Eq. (5), incorporating the equivalent moment of inertia from Eq. (6). The resulting deflection, δ_2, is verified against the serviceability limit: $\delta_2 \leq l/360$

3.5.3. Local Bending Capacity of Intermediate Panels

In triangular trusses with parallel web members, negative moments arise at orthogonal joints, similar to those observed at web openings in deep beams (see Figure 5). The bending resistance in these panel zones is evaluated using Eq. **Error! Reference source not found.**.

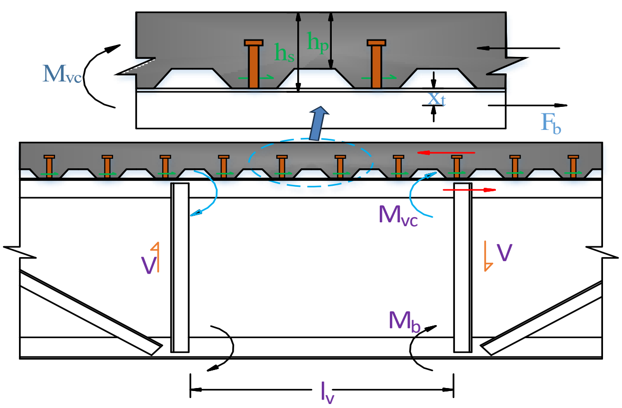

Figure 5. *Bending moment effect induced by shear forces from two web plates perpendicular to the flange plate*

$$M_v = M_{cv} + 2M_b\left(1 - \frac{T}{F_b}\right) + 2M_t \geq Vl_v \quad (9)$$

where M_{cv} is bending resistance due to composite action in the top chord; M_b is bending capacity of the bottom chord; M_t is bending capacity of the top chord; T is tensile force in the bottom chord; F_b is compressive capacity of the top chord, assumed to be entirely resisted by the concrete flange.

The concrete slab and the top flange of the truss function as a composite section through shear connectors, allowing interaction between materials. This composite behavior is characterized by a lever arm between the top flange and the mid-depth of the slab, multiplied by the shear force (F_q) transferred through stud connectors (see Figure 5).

$$M_{cv} \approx x_t + \frac{h_s + h_p}{2} F_q \quad (9)$$

3.5.4. Natural Frequency Check

To avoid perceptible vibrations, the following criterion as given in Eq. (10) is applied. Where δ_w is the deflection under 10% of design load.

$$f > 4Hz, f = \frac{18}{\sqrt{\delta_w}} \quad (10)$$

4. Application, results, and discussion

4.1. Probem statement

The initial structural system consists of an I-beam spanning 21 meters with a column spacing of 3 meters (see Figure 3). The floor system comprises a composite steel–concrete slab with a total thickness of 150 mm, including 100 mm of concrete topping and a 50 mm profiled steel deck (see Figure 6 and Figure 8). The shear connectors are ϕ22 mm in diameter with an initial length of 120 mm, reduced to 115 mm after welding.

Due to the large span and high self-weight of the I-beam, it is replaced in this study by a more efficient composite steel–concrete truss. Material specifications and applied loads are detailed in Table 2 and Table 3.

Table 2. *Applied loads (kN/m²)*

Load component	Construction stage	Service stage
Concrete slab self-weight	3.00	3.00
Steel decking	0.15	0.15
Slab reinforcement	0.04	0.04
Beam reinforcement	0.20	0.20
Ceiling	-	0.50
Total permanent load	**3.39**	**3.89**
Construction live load	0.50	-
Live load (occupants, equipment)	-	4.00
Partition load	-	1.00

Table 3. *Material Properties.*

Material	Grade	Property	Symbol	Value	Unit
Steel	S355	Yield strength	f_y	355	MPa
		Design strength	f_d	355 (γ = 1.06)	MPa
		Ultimate strength	f_u	510	MPa
		Young modulus	E_s	210	GPa
		Unit weight	γ_w	23.55	kN/m³
Concrete	C20/25	Characteristic strength	f_{ck}	20	MPa
		Young modulus	E_{cm}	29	MPa

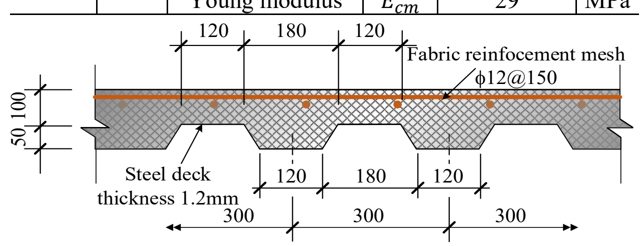

Figure 6. *Typical cross-section of a composite steel-concrete slab*

4.2. Preliminary selection of chord and bracing sections in composite steel–concrete trusses

4.2.1. Analysis of optimal cross-section selection

The selection of cross-sections for the top and bottom chords in composite trusses is critical for achieving both structural efficiency and material economy. Common options include T-sections, angle sections, and hollow structural sections (HSS):

T-sections, cut from standard I-sections, retain high structural efficiency while minimizing unused web material in long spans. They also simplify connection details by reducing the need for large gusset plates.

Angle sections, while easy to fabricate, tend to have limited strength due to their slenderness. Double-angle configurations often fail to meet the requirements for Class 1 sections under Eurocode 3, restricting their ability to develop full plastic moments.

Hollow Structural Sections (HSS) feature closed geometry, offering excellent stiffness and axial load resistance. Though more costly, they are ideal for demanding applications. Their wider diagonal spacing requires more refined connection detailing.

Conclusion: T-sections cut from I-profiles represent an optimal choice for high-rise floor systems, offering a balanced combination of structural performance, constructability, and cost-effectiveness.

Diagonal members are typically fabricated from single or double angle sections due to their simplicity in manufacturing and effective axial load transfer through straightforward connections.

4.2.2. Preliminary cross-section design for truss members

In this study, the internal forces in the truss members during the construction stage are used to preliminarily design member cross-sections in accordance with Eurocode 3 [13]. Based on Eurocodes EN 1990 [14] and EN 1991 [15], the fundamental load combination factors for the ultimate limit state (ULS) are $\gamma_G = 1.35$ for permanent loads and $\gamma_Q = 1.5$ for variable loads. The construction-stage load combination is therefore calculated using the data in Table 2 as follows:

$$q_n = \left(\gamma_G \cdot g_k + \gamma_Q \cdot q_k\right) \cdot b = \left(1.35 \cdot 3.39 + 1.5 \cdot 0.5\right) \cdot 3 = 15.98 kN/m \quad (11)$$

Since only the steel truss carries loads during the construction stage, the uniformly distributed load on the top chord is approximately converted into point loads applied at the top nodes (see Figure 7). Internal force analysis results from both analytical and numerical methods show close agreement and are illustrated in Figure 7.

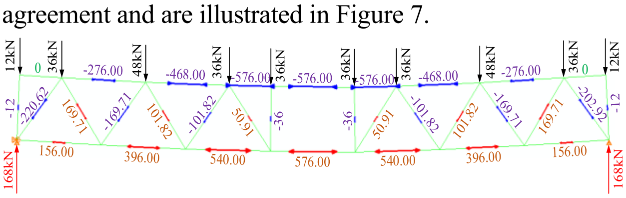

Figure 7. *Calculation diagram and internal force analysis results during the construction phase*

For member selection, the compressive forces shown in Figure 7 can be used in conjunction with appropriate effective lengths. Alternatively, buckling curves or analytical expressions may be applied. It is also important to preselect member dimensions to avoid excessive slenderness. In this study, compressive resistance is determined according to Eurocode 3 [13], using buckling curve "c". The resistance is computed assuming a partial safety factor (γ_M), although this may vary by country (typically 1.0 or greater).

Considering the importance of end connections in truss systems, vertical and diagonal members are selected to limit slenderness. Typically, a single-T section is used for the top chord, while a different profile is selected for the bottom chord to optimize strength and stiffness.

The preliminary cross-section design is based on internal force verification results presented in Table 4. For T-shaped top chords with constant sections, the effective buckling length in and out of plane is taken as $KL = 0.9L$, while for vertical and diagonal members $KL = 0.75L$, [13]. Compressive members must satisfy the buckling check: $N_{ed}/N_{b,Rd} \leq 1.0$ [13]. The design buckling resistance for cross-section classes 1, 2, and 3 is: $N_{b,Rd} = \chi A f_y / \gamma_{MI}$. For Class 4 sections: $N_{b,Rd} = \chi A_{eff} f_y / \gamma_{MI}$. The reduction factor is determined using Eq. (12).

$$\chi = \frac{1}{\Phi + \sqrt{\Phi^2 + \bar{\lambda}^2}} \leq 1.0 \quad (12)$$

The slenderness factor Φ and the dimensionless slenderness $\bar{\lambda}$ are determined using Eq. (13).

$$\begin{cases} \Phi = 0.5\left[1 + \alpha\left(\bar{\lambda} - 0.2\right) + \bar{\lambda}^2\right] \\ \left[\begin{array}{l} \bar{\lambda} = \sqrt{\dfrac{A f_y}{N_{cr}}} = \dfrac{L_{cr}}{i}\dfrac{1}{\lambda_1}, \text{with} \quad \lambda_1 = \pi\sqrt{\dfrac{E}{f_y}} \\ \bar{\lambda} = \sqrt{\dfrac{A_{eff} f_y}{N_{cr}}} = \dfrac{L_{cr}}{i}\dfrac{\sqrt{A_{eff}/A}}{\lambda}, \text{with} \quad i = \sqrt{\dfrac{I}{A}} \end{array}\right. \end{cases} \quad (13)$$

For tension members, the verification condition is: $N_{ed}/N_{t,Rd} \leq 1.0$ [13], where the design tensile resistance $N_{t,Rd}$ is the minimum of the gross section plastic resistance $N_{pl,Rd} = A f_y / \gamma_{M0}$ and Net section ultimate resistance $N_{u,Rd} = 0.9 A_{net} f_u / \gamma_{M2}$. Here, A_{net} is the gross cross-sectional area A minus the area of bolt holes. Verification results are summarized in Table 4.

Table 4. *Preliminary Cross-Section Data for Truss Members*

Members / Parameters	Top chord	Bottom chord	Tensile diagonal brace	compressive diagonal brace	vertical brace
f_{y0} (MPa)	335	335	335	335	335
N_0 (kN)	-576	576	169.71	-220.62	-36
KL (m)	2.70	-	-	1.31	0.81
Cross section type	$T175 \times 7 \times 10$	$T125 \times 6 \times 9$	$L60 \times 4$	$L100 \times 7$	$L50 \times 4$
A_0 (mm^2)	2905	1821	464	1351	384
c/t	17.5	13.89	15.00	14.29	12.50
$\bar{\lambda}$	0.73	-	-	0.73	1.46
Φ	0.90	-	-	0.89	1.87
χ	0.48	1.00	1.00	0.49	0.24
$\chi f_{y0} A_0$ (kN)	591.68	721.53	183.85	-277.81	-38.00

Note that the curve parameter α depends on the cross-section type and end conditions, as defined in Eq. (13): curve "a" ($\alpha = 0.21$) for excellent performance; curve "b" ($\alpha = 0.34$); curve "c" ($\alpha = 0.49$), commonly used for welded box sections or angle profiles; and curve "d" ($\alpha = 0.76$). This study adopts curve "c", with $\alpha = 0.49$.

The selected c/t ratios, ranging from 11.0 to 17.0, comply with Eurocode 3 [13] requirements. The T $200 \times 200 \times 12$ section is identified as the optimal choice due to its lighter weight and efficient connectivity with vertical and diagonal members. The selected bracing members offer sufficient load-bearing capacity, facilitate effective joint detailing, and ensure ease of construction and local stability. The final preliminary cross-section and its dimensions are shown in Figure 8.

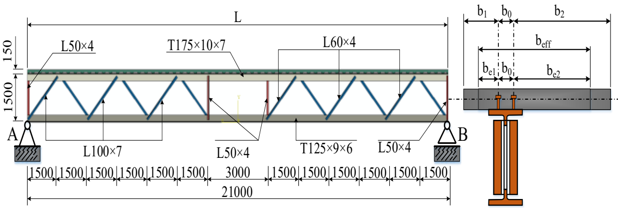

Figure 8. *Preliminary cross-section of the composite steel-concrete truss member*

4.3. Effective Width of the Concrete Flange

The effective width of the concrete flange is determined in accordance with Eurocode 4, as described in Section 3.1. The calculation follows the expressions provided in Table 1. The central flange width is taken as $b_0 = 0.1m$, and the side flange widths are determined as $b_1 = b_2 = B/2 = 3.0/2 = 1.5m$. The effective width coefficient β_i is given by: $\beta_i = 0.55 + 0.025 \times (L_e/b_{ei}) \leq 1.0$. On the other hand, the effective span is: $L_e = 0.85 \cdot L_1 = 0.85 \times 21 = 17.85m$. The effective widths b_{e1} and b_{e2} are both taken as: $b_{e1} = b_{e2} = 17.85/8 = 2.23m$, so both rounded to 1.5m. Thus, the effective width coefficient becomes: $\beta_1 = \beta_2 = 0.55 + 0.025 \times (17.85/1.5) = 0.85$. Finally, the total effective width is calculated as: $b_{eff} = 0.1 + 0.85 \times 1.5 + 0.85 \times 1.5 = 2.65m$.

4.4. Numerical method-based approach to problem solving in service stage

Based on the theoretical configuration of the composite steel–concrete truss established in accordance with Eurocode 4, a finite element model (FEM) was developed to complement the analytical results, enhance understanding of structural behavior, and improve the reliability of predictions. The FEM also enables the evaluation of detailed local responses of individual components, which are often beyond the scope of traditional analytical methods.

The geometry of the model follows the configuration illustrated in Figure 8. Steel is modeled using an elastoplastic material law governed by the von Mises yield criterion [16], while the concrete behavior is simulated using the Concrete Plastic Damage (CPD) model as defined by CEB-FIP 2010 [17]. Nonlinear analysis is carried out using an incremental–iterative Newton–Raphson algorithm [16].

The mesh comprises 8-node brick elements for all structural components except the steel deck, which is modeled using second-order 8-node shell elements with reduced integration to mitigate shear locking in thin plates. Perfect bond conditions are assumed between the concrete slab, the steel deck, and the upper chord of the steel truss. Boundary conditions consist of a pinned support at one end and a roller support at the other (see Figure 8). The complete finite element model is shown in Figure 9.

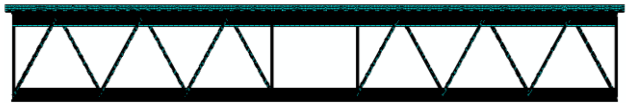

Figure 9. *Finite element analysis model*

4.5. Results and Discussion

4.5.1. Verification of the plastic moment capacity of the composite truss

According to Eurocode 4 [8], as discussed in Section 3.5, the condition for verifying the plastic moment capacity of a composite steel–concrete truss in the service stage is: $M^{+}_{pl,Rd} \geq M^{+(red)}_{Rd}$. The design bending resistance is calculated as: $M^{+(red)}_{Rd} = q_n l^2/8$, where q_n, derived from Eq. (11) and the service-stage loads in Table 2, equals $38.25\ kN/m$. Substituting the values yields: $M^{+(red)}_{Rd} = 2108.53\ kNm$.

The plastic moment resistance is determined from Eq. (3) using the following values: $F_{AB} = 721.53\ kN$, $F_{AT} = 1151.04\ kN$ (from Eq. (1)), and $F_C = 3003.33kN$ (from Eq. (2)). Since $F_{AB} + F_{AT} < F_C$, the plastic neutral axis is confirmed to lie within the concrete flange. Its location relative to the top surface of the concrete slab, calculated using Eq. (4), is: $z = 62.35\ mm$. Substituting all values into Eq. (3b), the resulting plastic moment resistance is: $M^{+}_{pl,Rd} = 1390.72kNm$. As this value is less than $M^{+(red)}_{Rd}$, the section does not meet the design requirement. Therefore, the cross-sections are revised to $T225 \times 8 \times 12$ for the upper flange and $T175 \times 7 \times 10$ for the lower flange. Upon re-evaluation, the updated plastic moment resistance is: $M^{+}_{pl,Rd} = 2171.89\ kNm$, which satisfies the verification condition.

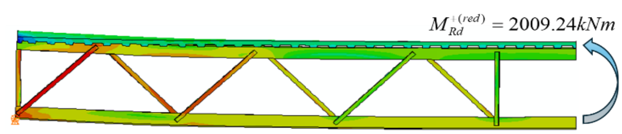

Figure 10. *Moment induced by the load* $q_n = 38.25\ kN/m$

Using these verified parameters, a finite element model of the composite steel–concrete truss is developed. The resulting bending moment distribution is shown in Figure 10. The discrepancy between the simplified beam assumption and the numerical simulation is 4.71%, primarily due to differences between the idealized and actual structural behavior.

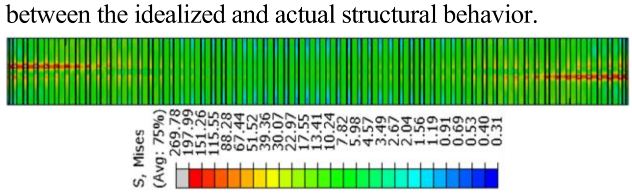

Figure 11. *Stress distribution in the steel deck*

The numerical model allows for a detailed analysis of each component within the composite truss, identifying critical regions and providing insights into localized behavior. This enables the development of optimized design solutions based on accurate stress distribution data. For example, the stress contours in the steel deck shown in Figure 11 highlight key performance features. Additional results, while significant, are beyond the scope of this paper.

4.5.2. Evaluation of deflection in the composite truss

The displacement is calculated using Eq. (5), with the equivalent moment of inertia determined from Eq. (6) as: $I_{eq} = 456862.58$ cm^4. The applied load, taken from Table 2, is: $q = 0.27$kN/cm, excluding load factors. The modulus of elasticity for steel is: $E_s = 21000$kN/cm^2. The truss span is modeled as a simply supported beam with: $L = 2100$cm. The computed displacement is: $\delta = -7.04$cm, while the allowable displacement at the service stage is: $[\delta] = L/360 = -5.83$cm, indicating non-compliance. To meet the serviceability limit, the cross-sectional dimensions of the top and bottom chords are increased to $T250 \times 10 \times 14$ and $T225 \times 8 \times 12$, respectively. With these revised sections, the equivalent moment of inertia becomes: $I_{eq} = 581999.67$cm^4. This results in a corresponding displacement of: $\delta = -5.53$cm, which satisfies the serviceability criterion. Numerical simulation yields a displacement of: $\delta = -5.56$cm, (see Figure 12), showing a deviation of only 0.54% compared to the theoretical value based on Eurocode 4. This close agreement confirms the consistency between analytical calculations and numerical simulations, ensuring the reliability of the proposed method for practical structural design.

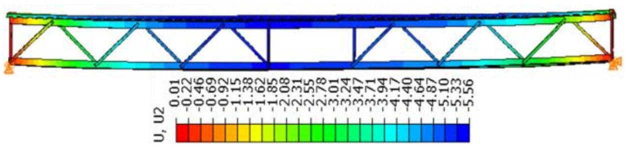

Figure 12. *Displacement due to Load in the Service Stage with $q = 27kN/m$*

5. Conclusion

This study presents a performance-based evaluation of long-span steel–concrete composite trusses for high-rise buildings, emphasizing their structural efficiency, material optimization, and suitability for modern construction practices. By integrating theoretical analysis with finite element modeling (FEM), the research demonstrates the superior load-bearing capacity, stiffness, and deflection control of composite trusses in comparison with conventional steel systems.

A major contribution of this work is the proposed method for preliminary cross-section selection during the construction stage, which streamlines early design iterations, reduces the need for extensive revisions, and improves both efficiency and constructability. This strategy accelerates project delivery timelines.

Furthermore, the validation of analytical predictions through numerical simulations affirms the reliability of composite truss behavior, offering practical design guidance for engineers and architects seeking high-performance structural solutions for tall buildings. The findings also support the refinement and broader adoption of Eurocode-based design practices, promoting the widespread implementation of composite systems in performance-driven engineering applications.

REFERENCES

[1] J. Shen, X. Zhang, P. Wu, K. Yue, and J. Chen, "Experimental and Finite Element Analysis of Bending Performance of Web-Embedded Double Inverted T-Shaped Steel–Concrete Composite Beams", *Buildings,* vol. 15, no. 5, p. 717, 2025, doi: https://doi.org/10.3390/buildings15050717.

[2] K.-Y. Xu, D. Xu, X.-T. Wang, T. Wang, J. Yan, and J.-B. Yan, "Seismic behaviors of steel truss-embedded steel-concrete composite shear walls", *Journal of Building Engineering,* vol. 49, p. 104112, 2022/05/15/ 2022, doi: https://doi.org/10.1016/j.jobe.2022.104112.

[3] A. B. Patricia Duratna, Jan Bujnak, "Analysis of the Behaviour of Steel-Concrete Composite Truss", *Komunikácie - vedecké listy Žilinskej univerzity v Žiline,* no. 4, pp. 46-50, 2011, doi: https://doi.org/10.26552/com.C.2011.4.46-50.

[4] J. Y. Richard Liew and H. Chen, "Direct analysis for performance-based design of steel and composite structures", *Progress in Structural Engineering and Materials,* vol. 6, no. 4, pp. 213-228, 2004, doi: https://doi.org/10.1002/pse.181.

[5] M. Tan, Y. Wu, W. Pan, G. Liu, and W. Chen, "Optimal Design of a Novel Large-Span Cable-Supported Steel–Concrete Composite Floor System", *Buildings,* vol. 14, no. 1, p. 113, 2024. [Online]. Available: https://www.mdpi.com/2075-5309/14/1/113.

[6] P. McKenna and R. M. Lawson, "Design of steel framed buildings for service integration", *SCI publication,* 1997. [Online]. Available: https://steelconstruction.info/images/7/70/SCI_P166.pdf.

[7] M. M. Ali and K. Al-Kodmany, "Structural Systems for Tall Buildings", *Encyclopedia,* vol. 2, no. 3, pp. 1260-1286, 2022. [Online]. Available: https://www.mdpi.com/2673-8392/2/3/85.

[8] EN 1994-1-1 (2004) (English): Eurocode 4: Design of composite steel and concrete structures–Part 1-1: General rules and rules for buildings, Comité-Européen-de-Normalisation, 2004. [Online]. Available: https://www.phd.eng.br/wp-content/uploads/2015/12/en.1994.1.1.2004.pdf

[9] R. P. Johnson and D. Anderson, "EN1994 Eurocode 4: design of composite steel and concrete structures", (in English), *Proceedings of the Institution of Civil Engineers. Civil Engineering,* vol. 144, pp. 33-38, 2001, doi: https://doi.org/10.1680/cien.2001.144.6.33.

[10] R. P. Johnson and D. Anderson, *Designers' Guide to EN 1994-1-1 Eurocode 4: Design of Composite Steel and Concrete Structures*. CPI Group (UK) Ltd, Croydon, CR0 4YY: Thomas Telford, 2004.

[11] S. Raji, K. Abdulraheem, R. Rahmon, and A. Adelowo, "Design of A Composite Truss System in A Multistorey Building", *Journal of Multidisciplinary Engineering Science and Technology (JMEST),* vol. 4, no. 3, pp. 6863-6870, 2017. [Online]. Available: https://www.jmest.org/wp-content/uploads/JMESTN42352097.pdf.

[12] A. Sharma, K. Pathak, and P. Singh, "Analytical comparison of composite and non-composite through type and deck type steel truss bridges", *Civil Engineering and Architecture,* vol. 9, no. 4, 2021, doi: https://doi.org/10.13189/cea.2021.090401.

[13] *EN 1993-1-1: Eurocode 3: Design of Steel Structures. Part 1-1: General Rules and Rules for Buildings*, CEN_(European-Committee-for-Standardization), Brussels, 2005. [Online]. Available: https://www.phd.eng.br/wp-content/uploads/2015/12/en.1993.1.1.2005.pdf

[14] *Eurocode - Basis of structural design*, CEN_(European-Committee-for-Standardization), Brussels, 2005. [Online]. Available: https://www.phd.eng.br/wp-content/uploads/2015/12/en.1990.2002.pdf

[15] *Eurocode 1: Actions on structures - Part 1-1: General actions Densities, self-weight, imposed loads for buildings*, CEN_(European-Committee-for-Standardization), Brussels, 2002. [Online]. Available: https://www.phd.eng.br/wp-content/uploads/2015/12/en.1991.1.1.2002.pdf

[16] M. Pham, N.-H. Dinh, C.-T. Dang, and H.-C. Truong, "Numerical Study of Bearing Strength of Infilled Concrete in Large Diameter CFST Column Reinforced by Shear Stoppers", *Designs,* vol. 8, no. 1, p. 9, 2024. [Online]. Available: https://www.mdpi.com/2411-9660/8/1/9.

[17] *Fib Model Code 2010*, 9783433604090, International-Federation-for-Structural-Concrete-(FIB), London, 2013/10/23 2010. [Online]. Available: https://onlinelibrary.wiley.com/doi/abs/10.1002/9783433604090.ch5